Molecular Dynamics Simulation of Heat Conduction through a Molecular Chain

Christian Schröder,*,† Vyacheslav Vikhrenko,‡ and Dirk Schwarzer§

Institute of Computational Biological Chemistry, University of Vienna, Vienna, Austria, Belarusian State Technological University, Minsk, Belarus, and Max-Planck-Institute for Biophysical Chemistry, Göttingen, Germany

Received: April 17, 2009; Revised Manuscript Received: September 14, 2009

This work deals with a molecular dynamics simulation analysis of the intramolecular vibrational energy transfer in a system of two chromophores, azulene and anthracene, bridged by an aliphatic chain and is motivated by corresponding laser experiments. After selective excitation of the azulene chromophore, the subsequent intramolecular vibrational energy redistribution is monitored by analyzing the transient temperatures of the two chromophores and the chain between them. The main focus concerns the heat conduction process in the chain. Therefore, the chain length was varied from 0 to 19 CH_2 units. In addition, methoxymethyl, 1,2-dimethoxyethyl, and a thiomethoxymethyl chains were studied. The investigation of the intramolecular vibrational energy process was decomposed into a temporal analysis and a spatial analysis. For short alkyl chains, the time constant of energy relaxation increases proportionally to the chain length. However, for longer chains, the time constant characterizing the energy decay of the azulene chromophore saturates and becomes independent of the chain length. This behavior is consistent with experimental findings. The spatial analysis shows more or less exponential decay of the temperature along the chain near the excited chromophore. In additional simulations, the two chromophores were thermostatted at different temperatures to establish a constant heat flux from the azulene to the anthracene side. The steady-state temperature profiles for longer alkyl chains show strong gradients near the two chromophores and constant but weak gradients in the central part of the chain. Both simulation methods indicate that strong Kapitza effects at the boundaries between each chromophore and the molecular chain dominate the intramolecular energy flux.

Introduction

Both intramolecular vibrational energy redistribution (IVR) and intermolecular vibrational energy transfer (VET) are of fundamental importance in gas- and condensed-phase chemical dynamics. These nonreactive elementary processes determine the rates, pathways, and efficiencies of chemical reactions. Whenever a polyatomic molecule is locally excited by some chemical or electromagnetic activation process, IVR provides the basic mechanism of energy exchange between different vibrational degrees of freedom (i.e., normal modes). Here, the term "local excitation" applies to the preparation of some zero-order eigenstates or superpositions thereof or even to a local distortion of the molecule. In the presence of a solvent bath, excess energy is transferred irreversibly to the bath degrees of freedom.[1,2] In addition, the solvent might affect the intramolecular redistribution of energy, which is usually taken into account by the notion of "solvent-assisted" IVR.[1,3−6] Whereas the assumption of rapid IVR (on the time scale of reactive processes) is at the heart of statistical unimolecular rate theories,[7,8] intermolecular equilibration determines the applicability of canonical transition state theory.[9] Often, a separation of time scales for IVR and VET is assumed, such as in Rice−Ramsberger−Kassel−Marcus Theory.[7] In the gas phase, where the average time between collisions is rather long, this assumption is usually correct, at least for low densities.[10,11] In solution, however, it is questionable in general.[1,5,12] Because IVR is driven by state-specific anharmonic couplings and because dissipative intermolecular energy transfer is a strongly frequency-dependent phenomenon, favoring VET by low-frequency vibrations, IVR might be incomplete on the time scale of energy-transferring collisions. In fact, in recent molecular dynamics simulations, this phenomenon was demonstrated for CH_2I_2 in $CDCl_3$ solvent.[12] For large molecules, where, because of the high density of states, IVR is often no longer strictly state-specific but statistical, the separability of time scales can usually safely be assumed even in liquid solution.[3,13,14]

Traditionally, IVR is discussed by reference to the eigenstate space of some zero-order molecular Hamiltonian.[15−17] The study of IVR has been extended to the investigation of vibrational energy transport between different chromophore parts of a large molecule through a flexible molecular chain.[4,18,19,20] In such a case, in addition to the energy and normal-mode picture, a (Cartesian) spatial dimension of IVR comes into play. In a series of experiments,[4,18] two chromophores are attached to an alkyl chain as illustrated in Figure 1. The first optical chromophore, azulene, is excited by a femtosecond laser pulse into its first excited singlet state, S_1, from which it returns via internal conversion within $\lesssim 1$ ps to the S_0 state,[21,22] creating a vibrationally highly excited ground-state azulene moiety. Subsequently, the excess energy flows through the alkyl chain to the second chromophore (e.g., benzene, 1-methylene anthracene, or anthracene).[23] The overall process can be monitored via transient absorption of photons from a second laser pulse tuned to the red edge of the azulene or the second chromophore (e.g., anthracene) spectra. From the change in the optical density, ΔOD, of the chromophores, the temperatures of the azulene and anthracene can be calculated.[4,23] In addition to IVR, the intramolecular energy flow is also characterized by a "harmonic dephasing" process of the eigenfrequencies of the used com-

* To whom correspondence should be addressed. E-mail: christian@mdy.univie.ac.at.
† University of Vienna.
‡ Belarusian State Technological University.
§ Max-Planck-Institute for Biophysical Chemistry.

10.1021/jp903546h
Published on Web 11/24/2009

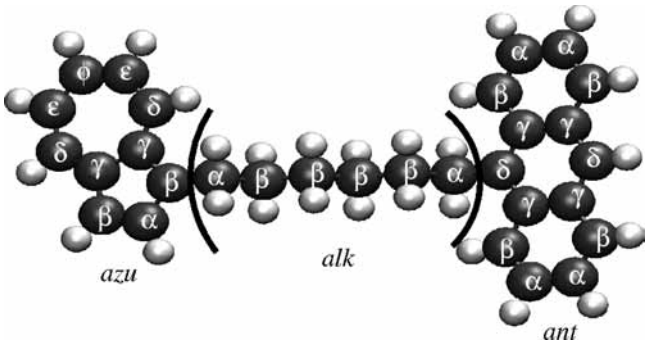

Figure 1. Definition of atom types in the azulene (azu) and anthracene (ant) moieties, as well as in the alkyl chain (alk). Hydrogen atoms are assigned the same Greek indices as the carbons to which they are bound.

pound. In a strict sense, this process is not IVR because, theoretically, no energy is transferred between the normal modes of the compound. However, because of the time scale of the experiment and the anharmonicities, the initial excited state is not restored. As a result, the harmonic dephasing (which occurs on a subpicosecond time scale) contributes to the energy transfer between the two chromophores within the experimentally accessible observation time. The IVR time constant is in the range of 1−5 ps depending on the length of the chain and the second chromophore,[23] whereas VET occurs with a time constant of approximately 20−50 ps in the molecular solvent used.[4,23] Because of the observed separation of time scales between IVR and VET, it can be assumed that IVR is complete on the time scale of VET. However, the VET time is remarkably close to the energy relaxation time of bare azulene in the same solvent,[21] which suggests that low-frequency vibrations of the bridged compounds are not significantly populated.[23]

Initial experimental data on azulene−anthracene compounds with short molecular bridges showed a linear dependence of the IVR time constant on the alkyl chain length.[4] These findings were confirmed by molecular dynamics simulations in which the interchromophore IVR time was found to be proportional to the alkyl chain length for up to four CH_2 units.[18] In principle, the linear dependence of the IVR time constant on the chain length can be explained by the Fourier law of heat conduction.[24] The two chromophores can be regarded as heat baths, which, however, because of their finite heat capacities, change their temperatures as a result of energy exchange with the bridge degrees of freedom. For a homogeneous one-dimensional spatial grid with end points that are held at different temperatures, Fourier's heat conduction equation yields a stationary solution with a linear temperature profile and, thus, a constant flux at all grid points. If the heat reservoir (end-point) temperatures vary in time but the reservoir heat capacities are still large as compared to that of the one-dimensional bridge, a similar nonequilibrium stationary state with an approximately linear temperature field is established, with a slope that decreases in the course of temperature equilibration.[4] As a result, Fourier's law predicts temperature equilibration times proportional to the length of the intervening spatial grid. Recent results, however, suggest a saturation of the interchromophore energy-transfer time for greater bridge lengths,[18] pointing to a possible breakdown of Fourier's law of heat conduction.

An "anomalous" thermal transport has also emerged from a large number of simulation studies on heat conduction in one-dimensional chains.[25,26] A major problem with these studies, however, is that the results strongly depend on the methods and the boundary conditions used.

Another type of anomalous thermal transport arises from the so-called Kapitza effect and has been examined experimentally and theoretically.[27−34] This effect appears at interfaces when system parameters are changing considerably, for example, at solid−liquid interfaces or at the contact of two crystallites in polycrystals.

In macroscopic theory, heat transfer across interfaces is taken into account by choosing proper boundary conditions,[35,36] such as by including a thermal resistance of the interface. In a microscopic description, the Kapitza effect is considered through a coordinate-dependent thermal conductivity that is larger in the bulk than in the boundary layers.

The aim of the present work is to investigate the heat conduction through an aliphatic chain between an azulene and an anthracene chromophore by means of nonequilibrium molecular dynamics simulations. This process is determined by anharmonic couplings between the vibrational degrees of freedom in the molecules. The electronic contribution to the heat transport can safely be ignored.

Two approaches are usually used for MD calculations of transport coefficients. One of them is based on linear response theory and the Green−Kubo relations that represent the transport coefficients through time integrals of the corresponding time correlation functions.[31,37,38] This approach is appropriate for spatially homogeneous systems because averaging over the system volume increases statistics by orders of magnitude. For spatially inhomogeneous systems, it is usually prohibitive because of problems with statistics.

In the other approach, a nonequilibrium system state is created, and transport coefficients are calculated as constants of proportionality between fluxes and gradients of the corresponding (thermodynamic) variables. In this approach, either time evolution of the system is considered, or a nonequilibrium steady state is created. Just nonequilibrium MD simulations were chosen in this work to investigate the energy-transfer problem.

This article is organized as follows: The next section describes the details of the simulations used to mimic the experimental situation. To reproduce the experimental data[18,23] for the azulene−anthracene system as closely as possible, a new molecular dynamics force field (presented in Appendix A) is introduced for these bridged compounds, which fits the experimental spectral information very well. The emphasis of this work lies on the spatial characterization of the IVR, that is, the IVR time constants of the two chromophores and the temperature profile within the alkyl chain. After a short introduction to the general concept of temperature and Fourier heat conduction, the necessity of introducing spatially dependent heat conductivity coefficients due to the "Kapitza" effect is explained. The presentation of the results is subdivided into two parts: First, the transient temperature relaxation is discussed, including the dependence on the chain length and chain composition. Additionally, one simulation series of azulene−$(CH_2)_3$−anthracene in Xe is presented. The spatial analysis deals with the spatial temperature profile in the case of the nonequilibrium simulations (emulating the laser experiments) and steady-state simulations with thermostatted chromophores. Finally, we summarize the results.

Simulation Details

In the present work, intramolecular vibrational energy redistribution in a model series of azulene−$(CH_2)_n$−anthracene compounds (cf. Figure 1) with varying alkyl chain lengths ($0 \leq n \leq 19$) is simulated via nonequilibrium classical molecular dynamics, mimicking the experimental pump/probe investiga-

tions performed on the same type of model systems.[4,18] In accordance with the interpretation of the experiments, the model systems are assumed to be equilibrated at a given heat bath temperature of the sample (usually 300 K, unless explicitly stated otherwise) prior to excitation by a subpicosecond visible light pulse. The latter is used in the experiments to locally excite the azulene chromophore into its lowest excited singlet state, S_1, from which the azulene unit returns to its S_0 state within $\leq$1 ps by internal conversion. Because local energy redistribution in the azulene chromophore cannot experimentally be separated from the internal conversion process, it is assumed that—on the time scale of through-bridge azulene-to-anthracene energy transfer—the initial vibrational excess energy is randomized among the azulene vibrations. Because of the relatively large number of local chromophore vibrational degrees of freedom, this local energy equilibrium (which is, in principle, microcanonical, with additional dispersive contributions due to canonical equilibrium prior to excitation) can be interpreted in terms of an initial nonequilibrium temperature applying to the local azulene degrees of freedom. Therefore, the initial mean excess energy of 2.23 eV (18000 cm^{-1}) is statistically distributed among the azulene vibrations according to a local canonical equilibrium. When vibrational degrees of freedom are treated classically, this heats the azulene to a temperature of approximately 850 K. Shortly thereafter, a coherent dephasing process transfers energy to the rest of the molecule on a subpicosecond time scale.[39] The delocalized energy heats the alkyl chain and anthracene by approximately 20−80 K and decreases the azulene temperature to 750 K.

Initialization of configurations in phase space was thus performed as follows: Starting from the minimum-energy geometries of model systems, the azulene was thermostatted at 750 K and the rest of the molecule at 320 K for a simulation period of 100 ps using a Nosé−Hoover algorithm of CHARMM.[40] This thermostatting avoids the "flying icecube" problem.[41] In other words, the thermostat does not introduce a translational drift. After this thermostatted phase, all thermostats were switched off. This ensured that there were no artificial Kapitza effects caused by the link between thermostatted and nonthermostated atoms in the system. The trajectory was propagated for an additional 150 ps using a time step of 0.1 fs. For each alkyl bridge length, an ensemble of 2000 such nonequilibrium trajectories was produced to ensure the statistical quality of the data.

The time scales of intramolecular energy redistribution will certainly depend on the shape of the potential energy surface. For large molecular systems as investigated in the present work, with more than 120−300 degrees of freedom, ab initio information on the energy surface even at low energies is beyond reach. Although simulation with ab initio forces calculated "on the fly" using efficient electronic structure methods have become increasingly popular,[42,43] the typical time scales covered are still in the lower picosecond range, which is too short for slow IVR. Therefore, we chose to rely on a local analytical force field, as traditionally employed in classical molecular dynamics simulations, parametrized to reproduce, as closely as possible, the spectrum of vibrational frequencies obtained from a combination of density functional theory (DFT) calculations and experimental information. As a result, the anharmonicity of the potential energy function and thus the detailed mode-to-mode couplings are, to some extent, "accidental". However, the usual functional forms of bond, angle, and torsional potentials are realistic enough to obtain a physically reasonable parametrization of the potential energy surface. Experience from previous simulation projects on IVR and VET in solution,[12] in particular the time scales obtained from molecular dynamics simulations as compared to experimental values, seems to justify our approach. The parametrization of the chromophores azulene (denoted as azu in the equations and tables) and anthracene (ant) and the alkyl chains (alk) is described in detail in Appendix A.

Temperature and Heat Conduction

In this work, many nonequilibrium MD simulations of azulene−anthracene systems were performed in order to juxtapose computational results and experimental data.[4,18,39] Because we want to concentrate on IVR within the molecule in this work, most of the simulation results deal with the pure azu−alk−ant derivatives without a solvent. Consequently, VET processes are neglected and not discussed here. The original experimental data consist of absorption−time profiles of the azulene and anthracene chromophores as a function of the length of the alkyl chain that bridges the two chromophores, as illustrated in Figure 1. This measured change in optical density, $\Delta OD(t)$, was been related to the temperature relaxation of the chromophores.[23] An assignment of individual temperatures $T_i(t)$ to each subunit $i \in \{azu, ant\}$ assumes that IVR in the chromophores is much faster than the energy redistribution between them through the aliphatic chain.

$T_i(t)$ is calculated in our simulations by summing the kinetic energies of the corresponding atoms j belonging to that subunit[25,44]

$$T_i(t) = \frac{1}{3n_i k_B} \sum_j^{n_i} m_j \left[\frac{d\mathbf{r}_j(t)}{dt}\right]^2 \quad (1)$$

where n_i is the number of atoms in the corresponding subunit. In accordance with the experiments, the chromophore temperatures $T_{azu}(t)$ and $T_{ant}(t)$ in the simulations relax, to a good approximation monoexponentially, to an equilibrium temperature T_{eq}

$$T_i(t) = \Delta T_i(t) + T_{eq} \quad (2)$$

$$= \Delta T_i(0) e^{-t/\tau_i} + T_{eq} \quad (3)$$

The time constants τ_i characterize the energy equilibration within the molecule and can be directly compared with experiment. After initial excitation, the local temperature of the azulene is far above T_{eq}. Hence, $\Delta T_{azu}(t)$ is positive. In contrast, $\Delta T_{ant}(t)$ is negative, because anthracene gains energy until T_{eq} is reached.

To elucidate the mechanism of heat transfer in detail, spatial temperature profiles through the molecular chain were calculated. To this end, the temperature $T(k,t) = T(x_k,t)$, with $x_k = kl$ for each CH_2 unit k, $0 \leq k \leq n$, was analyzed separately (l is the carbon−carbon bond length in the chain).

Based on a classic energy conservation equation for a chain in continuum representation

$$c_L \frac{\partial T(x,t)}{\partial t} + \frac{\partial J(x,t)}{\partial x} = 0 \quad (4)$$

the heat flux $J(x,t)$ distributes the local excess temperature until an equilibrium is achieved. In this equation, c_L is the specific heat per unit length. The classical way to describe the heat conduction is according to Fourier's law of heat conduction,[24]

which states that the heat flux, $J(x,t)$, is proportional to the temperature gradient

$$J(x,t) = -\kappa \frac{\partial T(x,t)}{\partial x} \tag{5}$$

The heat conduction coefficient κ and its inverse, the heat resistance $r = 1/\kappa$, are usually considered as constant. In this case, eq 5 results in a diffusive process of heat transfer with a uniform thermal diffusivity $\alpha = \kappa/c_L$. However, the molecular systems treated here are characterized by spatial inhomogeneities and hence require spatially varying heat resistances $r = r(x)$ and thermal diffusivities $\alpha(x) = [r(x)c_L]^{-1}$. In our classical system, the heat capacity can be approximated by $c_L = 9k_B l^{-1}$.

The heat flux can be determined by the power acting from one part of the molecule to another, i.e.:

$$J = \sum_j \mathbf{F}_j \cdot \mathbf{v}_j \tag{6}$$

Here, $\mathbf{v}_j$ is the velocity of the jth atom, and $\mathbf{F}_j$ is the sum of all forces acting on atom j due to the intramolecular potentials (bond, angle, dihedral, improper torsions) at the corresponding interface. Equation 6 can be used to calculate the heat flux at any bond in the alkyl chain.

Results and Discussion

We present our results in three sections. The first covers the transient temperature relaxation of the two chromophores after the initial excitation of azulene. This part closely resembles the experimental situation, and the corresponding time constants can be directly compared. The second part is concerned with the temperature profiles of the chain during relaxation. Finally, we discuss the results of simulations with chromophores thermostatted at different temperatures to establish a steady-state energy flux.

Time-Variant Temperature Relaxation. Because the attached optical chromophores azulene and anthracene are relatively large and the energy flux through the chain is relatively slow, local microcanonical equilibrium among their respective vibrational degrees of freedom can be described by an effective temperature, as in eq 1. The temperature was calculated for each subunit at each simulation step and averaged over the corresponding ensemble of trajectories.

We start our analysis with nonequilibrium simulations of azu−$(CH_2)_3$−ant in a bath of 225 Xe atoms. After initial excitation of the azulene, the energy was redistributed among all atoms of the azu−$(CH_2)_n$−ant compound via IVR and finally transferred to the heat bath. The corresponding temperature relaxation $T_i(t)$ is depicted in Figure 2. Likewise, we also calculated the temperature of the alkyl chain. However, as shown below, during relaxation, the vibrational degrees of freedom of the chain were not at all equilibrated, which makes the assignment of a temperature questionable. Rather, it can be understood as a measure of the internal energy of the chain.

The temperatures of azulene and anthracene can be well fitted by means of biexponential functions with equilibrium temperatures of 300 K. The longer time constant of approximately $\tau_{VET} = 100$ ps is attributed to the transfer of vibrational energy to the bath (VET) and is in reasonable agreement with the experimental τ_{VET} value of 35 ps.[23] The faster time constants, τ_{IVR}, attributed to the intramolecular energy flow turn out to be very similar to the values calculated for the isolated molecule

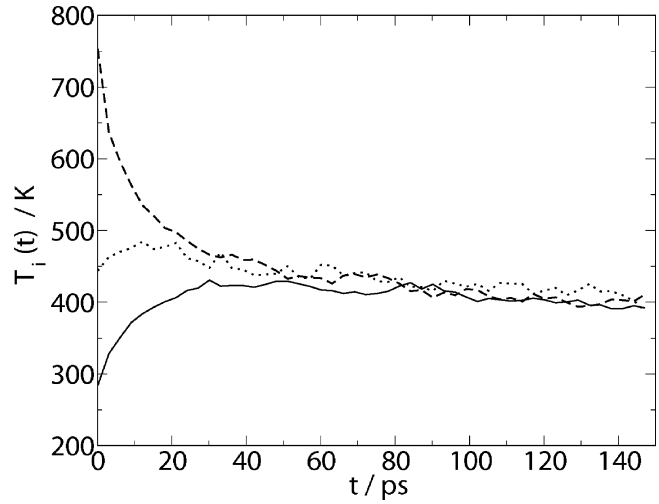

Figure 2. Ensemble-average temperature equilibration of azu−$(CH_2)_3$−ant dissolved in Xe. The temperature $T_i(t)$ was averaged over all atoms belonging to the subunit i. The dashed, dotted, and solid lines represent i = azu, alk, and ant, respectively.

without solvent; that is, the environment does not seem to influence the intramolecular process significantly. This is consistent with the experimental observation where no dependence of τ_{IVR} on the solvent was found.[23] Therefore, most of the calculations were done for the isolated molecules.

The results for the isolated azu−$(CH_2)_n$−ant model systems with $n = 0-19$ methylene units are presented in Figure 3. During IVR, the excess energy is transferred from the azulene to the rest of the molecule. Consequently, the temperature of the azulene decreases, and the temperatures of the chain and anthracene increase until T_{eq} is reached. Because the excess energy is redistributed solely among the atoms of the azu−$(CH_2)_n$−ant unit and not transferred to a heat bath, the equilibrium temperature T_{eq} is significantly higher than 300 K (cf. Figure 3). It decreases with chain length because of the increase in the heat capacity of the alkyl chain. For $n \geq 2$, the temperature dynamics of each azu−$(CH_2)_n$−ant compound in Figure 3b−f can be fitted monoexponentially according to eq 3. Molecules with directly linked chromophores or with just one methylene group between them ($n = 0, 1$) require a biexponential fit to model the energy equilibration. This is clearly visible in the case of azu−ant in Figure 3a. The time constants are summarized in Table 1. From the viewpoint of the intramolecular MD potential of these molecules, the azulene atoms are directly coupled to anthracene atoms by angle and dihedral potentials for $n < 2$. The number of potential terms affecting both chromophores is larger for $n = 0$ than for $n = 1$. This might explain why the time constant τ_2 is smaller for the species with $n = 0$. Experimentally,[4] a slow IVR component was not detected. However, the absolute value of τ_2 is in the same range as typical VET times, so that, even if present in the real molecular systems, it might be difficult to detect. Therefore, in the following discussion, only the faster component is considered and used for comparison with experiment.

In addition to the alkyl chains, a methoxymethyl chain and 1,2-dimethoxyethyl chain, as well as a thiomethoxymethyl chain, were analyzed. The substitution of a CH_2 unit with oxygen slows the IVR and increases the corresponding time constant by roughly 40%. This is consistent with the experimental data for the propyl and dimethylether compound.[18,23] Doubling the mass of the second unit in the chain by exchanging oxygen through sulfur further increases the IVR time constant by 40%. In one-

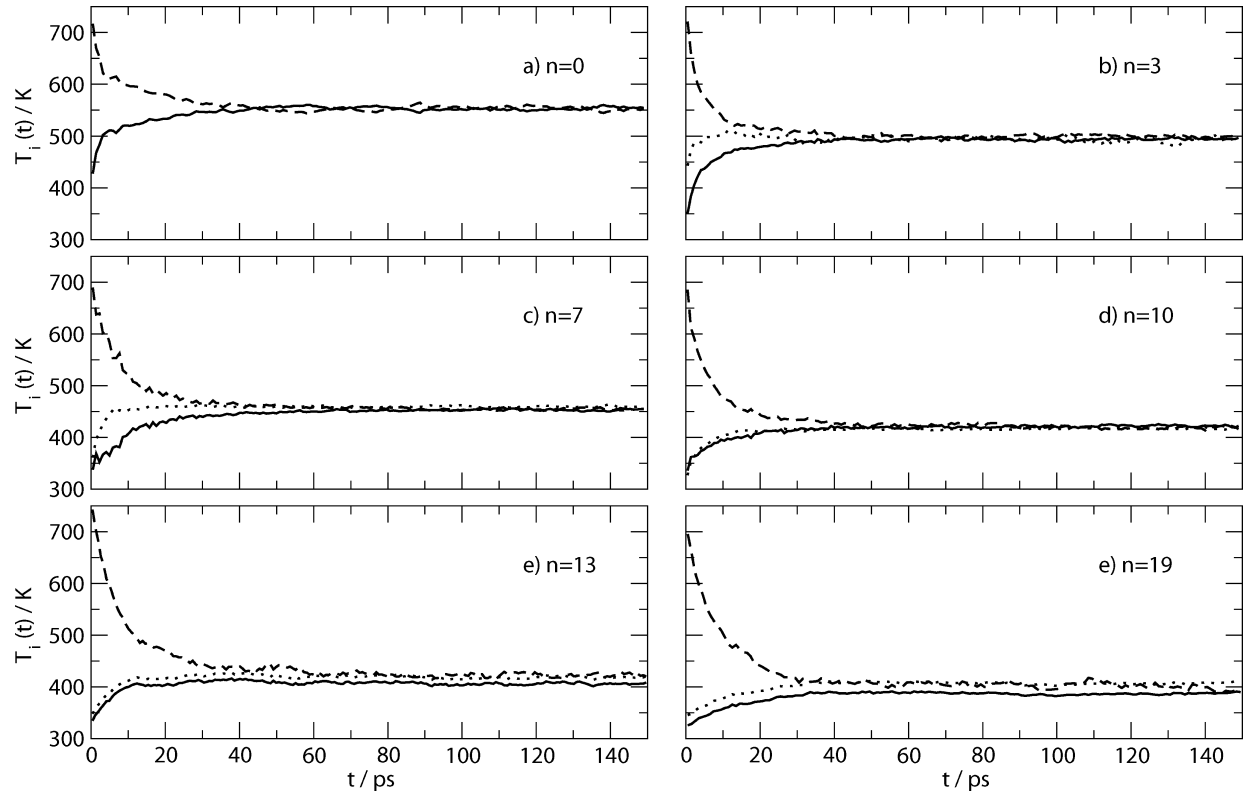

Figure 3. Ensemble-average temperature equilibration for isolated systems azu−$(CH_2)_n$−ant with varying n. The temperatures $T_i(t)$ of the units i = azu, alk, and ant are illustrated by dashed, dotted, and solid lines, respectively.

TABLE 1: Characteristic Intramolecular Energy-Transfer Times in Bridged Azulene−Anthracene Compounds[a,b]

	azu		ant	
$(CH_2)_n$	τ_1 (ps)	τ_2 (ps)	τ_1 (ps)	τ_2 (ps)
0	1.1 (0.8)	14.1	1.0	14.3
1	2.4 (2.0)	18.7	1.9	18.6
2	5.0 (3.7)		5.6	
3	5.8 (3.7)		7.1	
4	6.8		9.6	
5	6.9		8.3	
6	7.1 (4.2)		11.5	
7	7.9		11.6	
8	7.3		12.6	
9	7.4		14.0	
10	8.2		14.0	
13	8.1		15.1	
16	7.9		15.0	
19	8.8		17.0	
methoxymethyl ($n = 3$)	8.2 (5.0)		10.7	
thiomethoxymethyl ($n = 3$)	12.3 (5.1)		14.5	
1,2-dimethoxyethyl ($n = 6$)	9.5 (5.1)		15.5	

[a] Time constants for the azulene (azu) and anthracene (ant) sides were obtained from exponential fits. [b] Values in parentheses are experimental data.[4,18]

dimensional chain models, the mass effect was observed to be much more pronounced.[25] However, in our results, the interaction potentials of adjacent CH_2 units seem to attenuate the mass effect, and the deceleration of IVR seems to be caused by the smaller number of local modes transporting the energy through the chain and the reduced amplitudes of the local modes at the chromophore−chain interfaces.[39]

In Figure 4, the determined IVR time constants, τ_1, are plotted as a function of the alkyl chain length n and compared with experimental data. For long chains, the IVR rates derived from the simulations are roughly 50% slower than the experimental values. Nevertheless, the overall trend in the chain length dependence of τ_1, at least for the azulene component, is well reproduced by showing a saturation of τ_1 at alkyl bridge lengths with $n > 4$. For the anthracene moiety, this effect is less pronounced. We merely observe that the rise of τ_1 with n slows as the chain length continues to increase.

Transient and Steady-State Temperature Profiles. The observed plateaus in the experimental and simulated τ_1 values of azulene in Figure 4 suggest that they are dominated by similar energy-transfer mechanisms. The latter is analyzed here by studying the temperature profiles in the molecular chains during relaxation. This is exemplified in Figure 5 by means of the compound azu−$(CH_2)_{19}$−ant. The first and last circles in each graph refer to the azulene and anthracene temperatures, respectively. The circles between them belong to successive CH_2 units in the alkyl chain. The profiles were obtained 0.5 ps (black circles), 5 ps (gray circles), and 20 ps (white circles) after azulene excitation. The simulation data show that, during the whole relaxation process, a strong temperature gradient at the azu−alk interface persists, whereas in the chain and at the alk−ant interface, this gradient vanishes. Only for shorter chains (not shown here) are strong temperature gradients observed also at the alk−ant interface, indicating that the coupling of the chromophores to the alkane chain is limiting the energy transport. In the chain, the flux is obviously much faster. The strong temperature gradient at the azu−alk interface in Figure 5 extends to the fourth methylene group. This explains why the azulene relaxation time in Figure 4 reaches a plateau at $n > 4$.

Analogous nonlinear temperature profiles have often been found in computer simulations[30,31,45,46] of thermal conducting solids, for example, across grain boundaries in diamonds,[29] and are closely related to the so-called Kapitza resistance.[27,28] To investigate this effect in more detail and also determine a

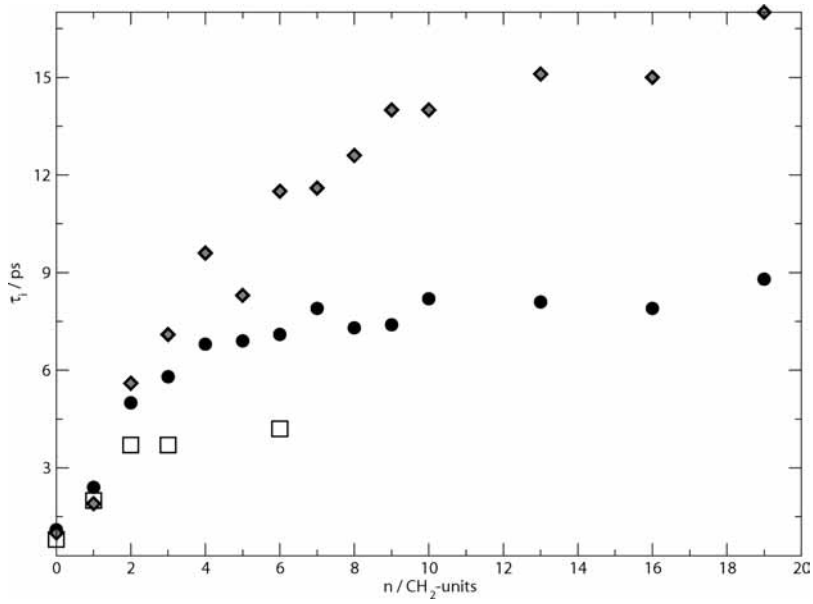

Figure 4. Energy loss and gain times for the azulene (full circles) and anthracene (gray diamonds) sides vs alkyl chain length (cf. Table 1). The squares represent the experimental values.[18]

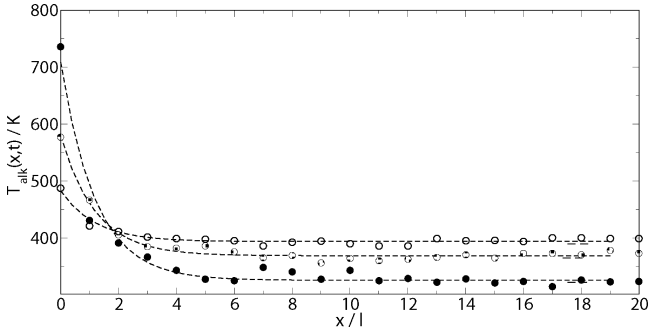

Figure 5. Transient temperature profiles of the alkyl chain of azu−$(CH_2)_{19}$−ant including azulene (left) and anthracene (right) after 0.5 ps (full circles), 5 ps (gray circles), and 20 ps (white circles). Monoexponential fits (dashed lines) provide the characteristic width of the Kapitza region at the azu−alk interface of 1.2 C−C bond length.

quantitative thermal transport parameter of the chain, steady-state simulations with thermostatted chromophores turn out to be more advantageous than calculations with transient excitation as presented so far.

For this purpose, the temperatures of azulene and anthracene were maintained at $T_{azu}(t) \approx 750$ K and $T_{ant}(t) \approx 320$ K, respectively, using a Nosé−Hoover thermostat with a response time of 0.1 ps. These values correspond to the chromophore temperatures of the simulations with transient excitation after harmonic dephasing before IVR starts. The steady-state temperature profiles are shown in Figure 6 for various values of n. In contrast to Figure 5, even for the longer bridges, temperature gradients in the chain and, in particular, at the alk−ant interface appear. We show below that the temperature gradient at the azu−alk Kapitza region is slightly larger than that at the alk−ant interface. Obviously, when a steady-state flux is not enforced, as is the case for the simulations with transient excitation, only the interface with the strongest gradient limits the energy flux and appears in the temperature profile (see Figure 5).

Because the steady-state heat flux J is independent of time and position, the spatially dependent heat resistance is easily derived by means of eq 5. The temperature profiles of Figure 6 suggest that the CH_2 chain be considered as being composed of three parts: two regions close to the chromophores, where the Kapitza effect is pronounced, and a central part, where the heat resistance is constant and equal to r_c, the resistance of the homogeneous chain far from its ends. The central part is absent for short chains, for which the Kapitza regions are superimposed on each other. Theoretical estimations[27,47] suggest that the Kapitza resistance decreases exponentially with the distance from the interphase. Thus, we model the heat resistance by

$$r(x) = [r_a e^{-x/\lambda_a}, r_c, r_b e^{-(L-x)/\lambda_b}] \tag{7}$$

where r_a, λ_a and r_b, λ_b are constants corresponding to azu and ant, respectively, and $L = (n + 1)l$ is the total chain length.

We require the heat resistance to be a continuous function of the coordinate x. Then, the temperature is a continuously differentiable function of x, and it is a simple task to find the boundaries, x_a and x_b, of the region with constant resistance r_c. They are defined as the points of the Kapitza regions where the spatial derivatives of temperature are equal to the constant temperature gradient in the central region.

The temperature profile is calculated by integrating the Fourier law

$$\frac{dT}{dx} = -r(x)J \tag{8}$$

at constant flux J. The results can be written for the three regions as

$$T_{alk}(x) = \left[\Delta T_a \frac{e^{-x/\lambda_a} - e^{-x_a/\lambda_a}}{1 - e^{-x_a/\lambda_a}} + T_a, \right.$$
$$\left. T_a + \overline{\nabla T}(x - x_a), T_b - \Delta T_b \frac{e^{-(L-x)/\lambda_b} - e^{-(L-x_b)/\lambda_b}}{1 - e^{-(L-x_b)/\lambda_b}}\right] \tag{9}$$

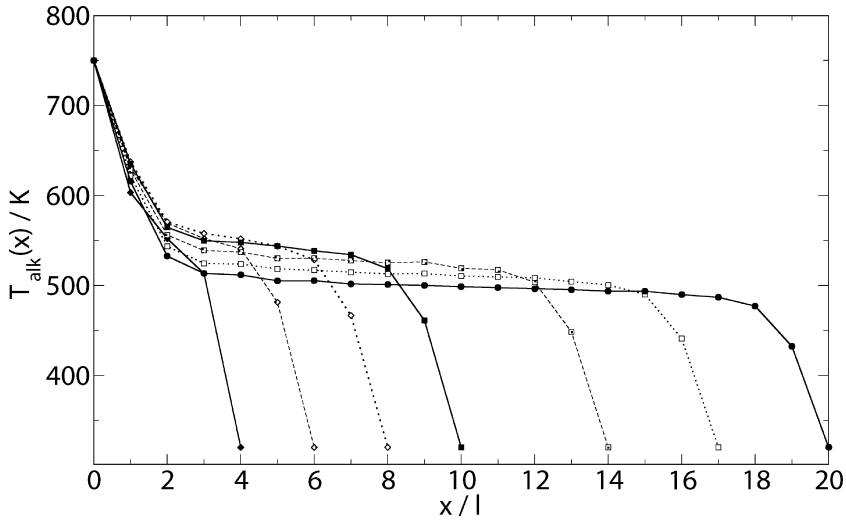

Figure 6. Steady-state temperature profiles of azu−$(CH_2)_{19}$−ant with $n = 3$, 5, 7, 9, 13, 16, and 19. The temperatures of the two chromophores were stabilized at 750 and 320 K, respectively, using Nosé−Hoover thermostats. The first circle ($x = 0$) corresponds to the azulene temperature; the last circle of each curve corresponds to the anthracene temperature.

where T_a and T_b are the temperatures of the boundaries of the constant-resistance region and

$$\Delta T_a = J\lambda_a[1 - \exp(-x_a/\lambda_a)]r_a,$$
$$\Delta T_b = J\lambda_b[1 - \exp(-(L - x_b)/\lambda_b)]r_b \qquad (10)$$

$$\Delta T_a = T_{azu} - T_a, \quad \Delta T_b = T_b - T_{ant}, \quad \overline{\nabla T} = -Jr_c \qquad (11)$$

It is worth to noting that the S-shaped steady-state temperature profiles cannot be explained by a temperature dependence of the heat conductivity. In this case, the derivative of eq 5 yields

$$\frac{d}{dx}\left[\kappa(T)\frac{dT}{dx}\right] = \frac{d\kappa}{dT}(\nabla T)^2 + \kappa(T)\frac{d^2T}{dx^2} = 0 \qquad (12)$$

The second derivative of the temperature has opposite signs near the chromophores. Thus, to satisfy eq 12, the temperature derivative of the thermal conductivity has to change its sign on the way from one chromophore to the other, which seems to be unrealistic.

The heat conduction equations (eqs 4, 5, and 7−9) are written for a continuous system, whereas we deal with a discrete chain model. Its grid points represent heat sources and reservoirs, and the bonds can be considered as heat resistances. The bond heat resistance is equal to the integral of $r(x)$ over the bond length. In the region of constant resistance, the bond resistance is $R_c = lr_c$. The Kapitza bond resistances near the azulene take the form

$$R_i = \int_{(i-1)l}^{il} r(x)\,dx = r_a\lambda_a[1 - \exp(-l/\lambda_a)]\exp[-(i - 1)l/\lambda_a] \qquad (13)$$

Because the Kapitza region extends up to five CH_2 units, a meaningful value of the bond resistance of the central chain can be evaluated only for alkyl chains with $n > 12$. The temperature profiles of Figure 6 for these long bridges show well-separated central segments with constant temperature gradients of -1.3 ± 0.1 K/l. The heat flux J was computed by means of eq 6 between every methylene unit during the steady-state simulations and averaged over all interfaces. Consistency of the data analysis was verified by comparing the different interfaces with respect to constant J. In Figure 7, the heat flux is plotted versus the total number of CH_2 units. With increasing chain length, the heat flux decreases up to a chain length of seven CH_2 units. Beyond this length, the heat flux is almost constant and reaches an average value to 21.6 nW. The qualitative trend of $J(n)$ is in accord with the dependence of the relaxation time on chain length found after transient excitation of azulene (see Figure 4). With J and the temperature gradients at hand, the central chain bond resistance and the total chain resistance can readily be calculated as $R_c = 1.3$ K/J = 0.06 K/nW and $R = (T_{azu} - T_{ant})/J = 20$ K/nW, respectively. For long chains, both quantities are independent of n.

Exponential fittings to the long-chain Kapitza regions yield $\lambda_a/l = 1.15 \pm 0.02$ at the azulene side and $\lambda_b/l = 0.97 \pm 0.02$ at the anthracene side. The temperature differences depend on the chain lengths: For $n = 19$, 16, and 13, respectively, we find $\Delta T_a = 253.3$, 240.2, and 226.3 K at the azulene side and ΔT_b =174.3, 189.3, and 206.9 K at the anthracene side. Thus, the asymmetry between the two sides of the chain is evident. It can be explained by the different natures and mode spectra of the two chromophores. A second reason might be the direction of the heat flux. To separate these two effects, steady-state simulations with identical chromophores on the two sides are in progress. The fitting constants are used to calculate the heat resistance of those bonds connecting the two chromophores with the chain. From eq 13, for $n = 19$, 16, and 13, respectively, we obtain values of 6.9, 6.5, and 6.2 K/nW at the azulene side and 5.2, 5.7, and 6.2 K/nW at the anthracene side. These numbers are 2 orders of magnitude larger than R_c in the center of the chain.

The thermal diffusivity of the chain in the region of constant heat conductivity is $\alpha_c = 1/(R_c c_L) = 3 \times 10^{-6}$ m^2/s (a C−C bond length of 0.15 nm was taken into account). This quantity can be compared with the thermal diffusivity of highly oriented polyethylene parallel to the draw direction, for which $\alpha_c = 9 \times 10^{-6}$ m^2/s was measured.[48] The reason for the difference might be that, in classical simulations, all vibrational modes are excited and contribute equally to the heat capacity whereas, in the polyethylene chain, high-frequency modes are not excited.

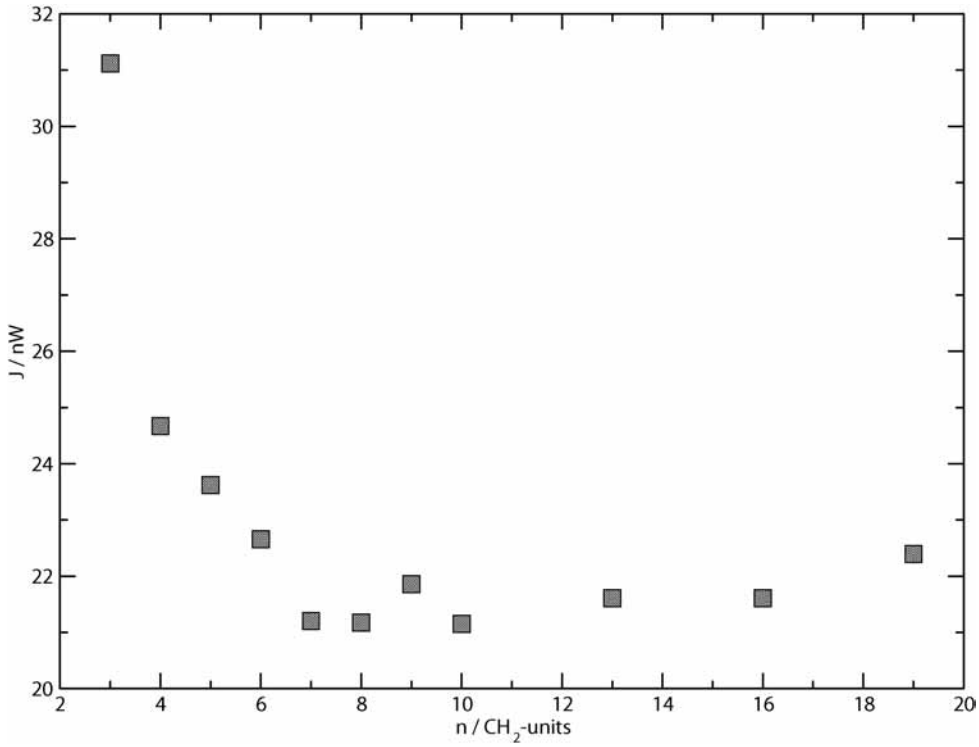

Figure 7. Average steady-state heat flux during the simulation with thermostatted chromophores as a function of alkyl chain length.

Hence, the average heat capacity c_L of a methylene unit is significantly smaller than assumed, such that α_c is underestimated.

Molecular dynamics simulations of heat conduction in solids[31,46,49−51] have shown strong Kapitza effects at the interface between thermostatted and nonthermostated regions. In principle, such artificial Kapitza effects could also be present in our simulations when the chromophores were thermostatted to establish a steady-state heat flux. The importance of this effect can be estimated by comparing the heat flux values of these simulations with those of our time-variant simulations, where, in the course of relaxation, no thermostats were used. The latter can be calculated according to $J = |dE_{azu}/dt| \simeq 51(k_B/\tau)\Delta T_{azu}(t)$, where the 51 degrees of freedom of azulene are considered and $\Delta T_{azu} \simeq 250$ K is the temperature difference between azulene and the alkyl chain in the steady-state simulations. With $\tau \simeq 8$ ps for the long chains (cf. Figure 4), the heat flux is calculated to be approximately 22 nW, which is very close to the value of 21.6 nW derived from the steady-state simulations. Therefore, we can conclude that, in our case, artificial Kapitza effects are of minor importance.

For heat transfer in strictly one-dimensional chains, another type of anomaly was reported.[25] In computer studies, the thermal conductivity of long but finite chains was found to diverge as n^β, where the coefficient β varies between 0.35 and 0.44. In our case, however, the chain is embedded in three-dimensional space. This might be the reason that the heat diffusivity and heat conduction coefficient for the long chains are constant and this effect is not observed.

Summary and Conclusions

In this study, vibrational energy transfer between the two chromophores azulene (azu) and anthracene (ant) connected by a molecular chain of variable length was investigated by classical MD simulations. The chain involves 0−19 methylene units; likewise, ether and thioether compounds were examined as well. In a first series of simulations, the relaxation toward intramolecular equilibrium after selective excitation of the azulene side was investigated. Analogous to a recent laser experiment, an excess energy of 18000 cm^{-1} was statistically distributed among the vibrational modes of the azulene unit. The subsequent energy flux through the bridge to the anthracene side was followed by monitoring of the temperatures of the two chromophores and each methylene unit. Comparison of the relaxation of azu−$(CH_2)_3$−ant in liquid xenon and under isolated conditions reveals that the influence of the solvent in the intramolecular energy flow is weak. Therefore, further analysis concentrated on simulations of these molecules in the gas phase.

For most of the molecules, the temperature drop at the azulene side could be modeled exponentially. The corresponding time constants are in the range of a few picoseconds and show a similar dependence on the number of methylene units n of the alkyl chain as in the corresponding laser experiments: For short bridges, the relaxation time increases proportionally to n, whereas for $n > 4$, it levels off and becomes independent of n. A closer analysis of the temperature profiles in these molecules indicates a pronounced Kapitza effect at the azulene−chain interface characterized by strong thermal resistances of the first few methylene units. As a result, the interface and not the remaining chain acts as a bottleneck for the energy drain of the excited azulene such that the corresponding time constants above $n = 4$ are independent of chain length.

To quantify the C−C bond resistances R_c in the alkyl bridges, additional calculations with thermostatted chromophores were performed, providing steady-state temperature profiles with constant energy flux. It was found that, on both sides, R_c decreases exponentially with the distance from the chromophore and levels off at the fifth methylene unit. For long chains (i.e., $n > 12$), a domain with constant R_c is observed in the center of the bridge. Here, the bond resistance is 2 orders of magnitude smaller than at the edges of the Kapitza regions. Contrary to true one-dimensional chains, the heat conductivity coefficient in the bridge center does not depend on chain length, probably

because our model systems are embedded in three-dimensional space. The resulting heat diffusivity compares reasonably well with that of highly oriented polyethylene in the draw direction. It is shown that the observed temperature profiles cannot be explained by a temperature dependence of the heat conductivity and that artificial Kapitza effects at the thermostat−chromophore interface are of minor importance.

Acknowledgment. C.S. thanks Prof. O. Steinhauser and Dr. A. Svrcek-Seiler for very helpful discussions. The authors thank one of the reviewers for constructive criticism and suggestions. Financial support of this project by the Deutsche Forschungsgemeinschaft (SFB "Molekulare Mechanismen unimolekularer Prozesse") is gratefully acknowledged.

Appendix A

Parameterization

Parameterization of the force field in terms of bond, angle, and dihedral potentials was first done separately for the two chromophores (azu, ant) and the saturated chain (alk), taking advantage of the smaller number of normal modes to be adjusted for the subunits, where azulene, anthracene, and butane served as the respective model bases. In a second step, the interfacial bonding potentials at the azu−alk and alk−ant boundaries were determined so as to reproduce the theoretical normal-mode spectrum of the bridged azu−alk−ant molecule. The normal-mode vibrational frequencies of subunits and bridged molecules were computed by the B3LYP method within DFT using the Gaussian 98 program package[52] and scaled by the empirical factor 0.9613.[53] It turned out that neither the intrachromophore and intrachain potentials nor the interfacial force field needed to be changed in order to reasonably reproduce the theoretical mode spectra. This has the additional advantage that a systematic comparison of energy redistribution in bridged bichromophoric molecules of varying alkyl chain length is possible without having to consider possible effects of changes in the force-field parameters on the time scales and mechanism of IVR.

Atomic partial charges as obtained from the Gaussian 98 program output were not used in the molecular dynamics simulations, because (long-range) polar interactions were not regarded as essential for IVR in the isolated molecules studied here and for intermolecular energy transfer in xenon solvent. The inclusion of intramolecular van der Waals interactions did not change the simulation results significantly for a subset of samples with varying chain length. Therefore, in the systematic variation of alkyl chain length, these types of potentials were omitted in order to additionally enhance the simulation speed. However, we also simulated the azu−$(CH_2)_3$−ant system in 225 Xe atoms in order to analyze the interplay of IVR and VET in our systems. In this case, we used the Lennard-Jones parameters $\sigma = 4.055$ Å and $\varepsilon = 0.457$ kcal/mol for the interaction of the carbon atoms with Xe. Furthermore, these nonbonded interactions complicate the parametrization with respect to the normal modes because strong intermolecular potentials shift the normal modes to lower frequencies (even imaginary frequencies were detected). In addition to the parametrization, the interpretation of the IVR is much more complicated. Because of the nonbonded interactions, parts of the excess energy of the hot azulene are transferred to the anthracene without taking the path through the alkyl bridge. Another reason concerns the analysis of the heat current. In future equilibrium simulations, we plan to evaluate the heat flux through the chain directly. A detailed Green−Kubo analysis seems far to complex if each chain atom interacts with all other atoms in the system.

TABLE 2: Force Field of Azulene[a]

Bonds		
	k_r [kcal/(mol Å^2)]	r_0 (Å)
$C_\alpha-C_\beta$	400	1.395
$C_\beta-C_\gamma$	400	1.396
$C_\gamma-C_\gamma$	400	1.487
$C_\gamma-C_\delta$	300	1.386
$C_\delta-C_\varepsilon$	300	1.388
$C_\varepsilon-C_\phi$	300	1.389
$H_\alpha-C_\alpha$	360	1.069
$H_\beta-C_\beta$	360	1.068
$H_\delta-C_\delta$	360	1.072
$H_\varepsilon-C_\varepsilon$	360	1.072
$H_\phi-C_\phi$	360	1.074

Angles		
	k_θ [kcal/(mol rad^2)]	θ_0 (deg)
$C_\beta-C_\alpha-C_\beta$	80.0	109.8
$C_\alpha-C_\beta-C_\gamma$	80.0	108.5
$C_\beta-C_\gamma-C_\gamma$	60.0	106.6
$C_\beta-C_\gamma-C_\delta$	43.3	126.2
$C_\gamma-C_\gamma-C_\delta$	43.3	127.3
$C_\gamma-C_\delta-C_\varepsilon$	80.0	129.2
$C_\delta-C_\varepsilon-C_\phi$	80.0	128.6
$C_\varepsilon-C_\phi-C_\varepsilon$	80.0	130.0
$H_\alpha-C_\alpha-C_\beta$	32.0	125.1
$H_\beta-C_\beta-C_\alpha$	35.0	126.2
$H_\beta-C_\beta-C_\gamma$	35.0	125.3
$H_\delta-C_\delta-C_\gamma$	37.0	115.3
$H_\delta-C_\delta-C_\varepsilon$	37.0	115.8
$H_\varepsilon-C_\varepsilon-C_\delta$	33.0	115.8
$H_\varepsilon-C_\varepsilon-C_\phi$	33.0	115.7
$H_\phi-C_\phi-C_\varepsilon$	30.0	115.0

Dihedrals			
	A (kcal/mol)	m	δ (deg)
$C_\alpha-C_\beta-C_\gamma-C_\delta$	7.0	2	−180.0
$C_\beta-C_\alpha-C_\beta-C_\gamma$	6.0	2	−180.0
$C_\gamma-C_\delta-C_\varepsilon-C_\phi$	1.0	2	−180.0
$C_\delta-C_\varepsilon-C_\phi-C_\varepsilon$	3.0	2	−180.0
$C_\beta-C_\gamma-C_\gamma-C_\beta$	1.0	2	−180.0
$C_\beta-C_\gamma-C_\gamma-C_\delta$	1.0	2	−180.0
$C_\delta-C_\gamma-C_\gamma-C_\delta$	4.0	2	−180.0
$C_\beta-C_\gamma-C_\delta-C_\varepsilon$	7.5	2	−180.0
$C_\alpha-C_\beta-C_\gamma-C_\gamma$	7.0	2	−180.0
$C_\gamma-C_\gamma-C_\delta-C_\varepsilon$	3.0	2	−180.0
$H_\beta-C_\beta-C_\gamma-C_\delta$	1.3	2	−180.0
$H_\beta-C_\beta-C_\alpha-C_\beta$	6.3	2	−180.0
$H_\delta-C_\delta-C_\gamma-C_\beta$	2.3	2	−180.0
$H_\delta-C_\delta-C_\varepsilon-C_\phi$	1.3	2	−180.0
$H_\alpha-C_\alpha-C_\beta-C_\gamma$	5.3	2	−180.0
$H_\phi-C_\phi-C_\varepsilon-C_\delta$	2.0	2	−180.0
$H_\varepsilon-C_\varepsilon-C_\delta-C_\gamma$	1.3	2	−180.0
$H_\varepsilon-C_\varepsilon-C_\phi-C_\varepsilon$	1.0	2	−180.0
$H_\phi-C_\phi-C_\varepsilon-H_\varepsilon$	2.0	2	−180.0

Improper Torsions		
	k_Φ [kcal/(mol rad^2)]	Φ_0 (deg)
$C_\alpha-C_\beta-C_\beta-H_\alpha$	30.0	0.0
$C_\beta-C_\alpha-C_\gamma-H_\beta$	30.0	0.0
$C_\delta-C_\gamma-C_\varepsilon-H_\delta$	30.0	0.0
$C_\varepsilon-C_\delta-C_\phi-H_\varepsilon$	30.0	0.0
$C_\phi-C_\varepsilon-C_\varepsilon-H_\phi$	30.0	0.0

[a] Potential energy functions have the forms $V(r) = 0.5k_r(r - r_0)^2$, $V(\theta) = 0.5k_\theta(\theta - \theta_0)^2$, $V(\Phi) = A[1 + \cos(m\Phi - \delta)]$, and $V(\Phi) = 0.5k_\Phi(\Phi - \Phi_0)^2$ for the bonds, angles, dihedral angles, and improper torsions, respectively.

TABLE 3: Fundamental Vibrational Frequencies of Azulene Extracted from Experimental Data ($\tilde{\nu}_{exp}$), DFT/B3LYP Calculations ($\tilde{\nu}_{DFT}$), and the Force Field ($\tilde{\nu}$) of Table 2

no.	$\tilde{\nu}_{exp}$ (cm^{-1})	$\tilde{\nu}_{DFT}$ (cm^{-1})	$\tilde{\nu}$ (cm^{-1})	no.	$\tilde{\nu}_{exp}$ (cm^{-1})	$\tilde{\nu}_{DFT}$ (cm^{-1})	$\tilde{\nu}$ (cm^{-1})	no.	$\tilde{\nu}_{exp}$ (cm^{-1})	$\tilde{\nu}_{DFT}$ (cm^{-1})	$\tilde{\nu}$ (cm^{-1})
1	189	157	194	17	900	842	866	33	1378	1365	1399
2	240	164	229	18	911	880	867	34	1396	1372	1420
3	304	308	318	19	941	904	914	35	1443	1429	1480
4	323	325	330	20	952	924	926	36	1448	1431	1496
5	331	395	395	21	965	937	967	37	1457	1473	1528
6	406	413	429	22	971	954	970	38	1480	1519	1578
7	486	479	434	23	987	960	1002	39	1536	1570	1598
8	542	552	514	24	1012	983	1016	40	1579	1580	1642
9	562	588	552	25	1049	1023	1027	41	2968	3008	3028
10	680	653	572	26	1058	1039	1030	42	3018	3010	3029
11	712	696	583	27	1117	1140	1042	43	3037	3018	3031
12	731	712	745	28	1160	1190	1067	44	3037	3036	3035
13	762	715	759	29	1210	1195	1130	45	3042	3045	3036
14	795	752	765	30	1216	1250	1175	46	3072	3072	3036
15	813	764	785	31	1268	1271	1224	47	3077	3090	3036
16	825	801	858	32	1300	1284	1297	48	3098	3098	3039

Although short-range repulsive potentials are certainly necessary for a proper description of coiled conformations at large bridge lengths, in the present study, the alkyl chain was always initialized in its zigzag-type all-trans conformation regarded as the global conformational energy minimum,[54,54] where, on the simulation time scale (up to 150 ps), the conformational energy barriers effectively prevent transitions to coiled conformations with a sandwich-like chromophore−chromophore configuration. Exclusion of such configurations ensures that interchromophore vibrational energy transport in the simulations must necessarily take place across the alkyl bridge. Although sandwich-like structures cannot rigorously be excluded in the experiments, such conformations are entropically disfavored, and the strength of bonding potentials as compared to van der Waals interactions suggests that, even for sandwich-like conformations, IVR is the basic mechanism of interchromophore energy transfer.

DFT/B3LYP calculations of the minimum-energy geometry and vibrational normal-mode frequencies of isolated azulene were performed using a 6-311++g(3df,3pd) basis set. The C_{2v} symmetry of azulene allows for the definition of six types of carbon atoms (Greek indexes α, β, γ, δ, ε, ϕ) and five types of hydrogen atoms (indexes α, β, δ, ε, ϕ), as illustrated in Figure 1. Although connection of the alkyl chain to one of the C_β atoms destroys the C_{2v} symmetry, the atom types of Figure 1 are retained also for the bridged compounds. Table 2 contains the parameters for bond, angle, and dihedral potentials of the azulene moiety as obtained from the adjustment to the normal-mode spectrum. Whereas force-field parameters for bond and angle potentials were taken from ref 56, torsional potentials were slightly refined. In addition to cosine-type dihedral potentials, quadratic ("harmonic") torsional potential functions had to be employed to prevent large-amplitude out-of-plane hydrogen motions. Table 3 compares the theoretical vibrational normal-mode frequencies from DFT to the experimental fundamental frequencies. The parametrization of the isolated anthracene force field was based on DFT calculations using a 6-311G** basis set in combination with experimental spectral data.[57] As a result of the D_{2h} symmetry of anthracene, four types of carbon and three types of hydrogen atoms suffice to define the local force field in Figure 1. Table 4 contains the parameters for bond, angle, and cosine-type dihedral potentials of the anthracene molecule. In Table 5, the experimental and theoretical (DFT) vibrational frequencies are collected. For parametrization of the alkyl-chain force field, the butane molecule served as the basic model, because it is the smallest linear alkane containing all relevant local interactions and potentials relevant for shorter as well as longer alkyl bridges, including a CC−CC internal rotation (torsion). As

TABLE 4: Force Field of Anthracene[a]

Bonds		
	k_r [kcal/(mol Å^2)]	r_0 (Å)
$C_\alpha-C_\alpha$	292.5	1.425
$C_\alpha-C_\beta$	292.5	1.367
$C_\beta-C_\gamma$	292.5	1.429
$C_\gamma-C_\delta$	292.5	1.398
$C_\gamma-C_\gamma$	292.5	1.443
$H_\alpha-C_\alpha$	397.5	1.084
$H_\beta-C_\beta$	397.5	1.084
$H_\delta-C_\delta$	397.5	1.086
Angles		
	k_θ [kcal/(mol rad^2)]	θ_0 (deg)
$C_\alpha-C_\beta-C_\gamma$	75.0	120.8
$C_\beta-C_\gamma-C_\delta$	75.0	121.7
$C_\gamma-C_\delta-C_\gamma$	75.0	121.0
$C_\beta-C_\gamma-C_\gamma$	75.0	118.8
$C_\delta-C_\gamma-C_\gamma$	75.0	119.5
$C_\alpha-C_\alpha-C_\beta$	75.0	120.4
$H_\alpha-C_\alpha-C_\beta$	38.5	121.0
$H_\alpha-C_\alpha-C_\alpha$	38.5	118.6
$H_\beta-C_\beta-C_\alpha$	38.5	121.2
$H_\beta-C_\beta-C_\gamma$	38.5	118.1
$H_\delta-C_\delta-C_\gamma$	38.5	119.5
Dihedrals		
	A (kcal/mol)	m	δ (deg)
$C_\alpha-C_\beta-C_\gamma-C_\delta$	5.6	2	−180.0
$C_\beta-C_\gamma-C_\delta-C_\gamma$	5.6	2	−180.0
$C_\gamma-C_\beta-C_\alpha-C_\alpha$	5.6	2	−180.0
$C_\beta-C_\alpha-C_\alpha-C_\beta$	5.6	2	−180.0
$C_\alpha-C_\beta-C_\gamma-C_\gamma$	5.6	2	−180.0
$C_\beta-C_\gamma-C_\gamma-C_\beta$	5.6	2	−180.0
$C_\beta-C_\gamma-C_\gamma-C_\delta$	5.6	2	−180.0
$C_\delta-C_\gamma-C_\gamma-C_\delta$	5.6	2	−180.0
$H_\alpha-C_\alpha-C_\beta-C_\gamma$	7.4	2	−180.0
$H_\alpha-C_\alpha-C_\alpha-C_\beta$	7.4	2	−180.0
$H_\beta-C_\beta-C_\alpha-C_\alpha$	7.4	2	−180.0
$H_\beta-C_\beta-C_\gamma-C_\delta$	7.4	2	−180.0
$H_\delta-C_\delta-C_\gamma-C_\beta$	7.4	2	−180.0
$H_\alpha-C_\alpha-C_\beta-H_\beta$	7.4	2	−180.0
$H_\alpha-C_\alpha-C_\alpha-H_\alpha$	7.4	2	−180.0

[a] Potential energy functions have the forms $V(r) = 0.5k_r(r - r_0)^2$, $V(\theta) = 0.5k_\theta(\theta - \theta_0)^2$, and $V(\Phi) = A[1 + \cos(m\Phi - \delta)]$ for the bonds, angles, and dihedral angles, respectively.

TABLE 5: Fundamental Vibrational Frequencies of Anthracene Extracted from Experimental Data ($\tilde{\nu}_{exp}$), DFT/B3LYP Calculations ($\tilde{\nu}_{DFT}$), and the Force Field ($\tilde{\nu}$) of Table 4

no.	$\tilde{\nu}_{exp}$ (cm^{-1})	$\tilde{\nu}_{DFT}$ (cm^{-1})	$\tilde{\nu}$ (cm^{-1})	no.	$\tilde{\nu}_{exp}$ (cm^{-1})	$\tilde{\nu}_{DFT}$ (cm^{-1})	$\tilde{\nu}$ (cm^{-1})	no.	$\tilde{\nu}_{exp}$ (cm^{-1})	$\tilde{\nu}_{DFT}$ (cm^{-1})	$\tilde{\nu}$ (cm^{-1})
1	106	92	111	23	852	846	821	45	1346	1376	1422
2	126	121	174	24	858	867	837	46	1384	1414	1435
3	234	235	212	25	879	897	921	47	1400	1415	1449
4	244	236	308	26	903	913	944	48	1412	1428	1460
5	287	269	339	27	908	919	963	49	1450	1482	1465
6	380	388	353	28	916	929	991	50	1460	1487	1507
7	397	396	358	29	956	968	1018	51	1480	1517	1520
8	397	398	379	30	958	973	1027	52	1542	1579	1543
9	469	480	428	31	977	995	1053	53	1561	1594	1544
10	479	485	440	32	988	996	1074	54	1596	1625	1549
11	491	506	495	33	998	1026	1100	55	1627	1669	1551
12	522	536	538	34	1007	1031	1105	56	1632	1671	1645
13	580	591	549	35	1098	1127	1106	57	3017	3154	3180
14	603	618	594	36	1124	1159	1188	58	3022	3156	3180
15	625	642	601	37	1151	1174	1214	59	3027	3158	3182
16	652	662	602	38	1164	1189	1219	60	3048	3159	3182
17	726	741	649	39	1167	1190	1240	61	3052	3163	3182
18	743	759	659	40	1187	1210	1285	62	3054	3164	3184
19	754	763	684	41	1264	1290	1387	63	3067	3176	3185
20	760	770	769	42	1272	1291	1393	64	3071	3176	3185
21	773	783	784	43	1273	1294	1393	65	3072	3188	3187
22	809	821	796	44	1318	1339	1400	66	3084	3188	3187

indicated in Figure 1c, only two types of carbon and hydrogen atoms were used in the molecular dynamics force field. Terminal carbons were denoted by the index α, whereas all other carbons were assumed to be equivalent with respect to their relevant local interactions and were assigned the index β. As for the chromophore moieties, hydrogen atoms were assigned the same Greek indexes as the carbons to which they were bound, and thus all nonterminal (β) hydrogens were assumed to be equivalent. See below for a justification of this assumption.

Goodman[54] and Allinger et al.,[55] by using an MMFF force field,[58] identified the all-trans (zigzag-type) conformation as the global energy minimum for linear alkanes of up to 17 and 24 methylene units, respectively. Therefore, we assumed that, for alkyl chains of up to 19 CH_2 increments, as employed in the present model series, the all-trans form is the most stable one, dominating the conformational ensemble. A systematic investigation of conformational statistics was not performed here. Investigation of the effects of different alkyl-bridge conformations on the interchromophore IVR is hence postponed to future studies. Starting from a *trans*-butane geometry optimized using DFT/6-311G**, additional methylene units were added, retaining the all-trans conformation, and the resulting structure was optimized (DFT/6-311G**). As it turns out, the geometrical parameters (equilibrium bond lengths and angles) changed only slightly upon addition of one additional CH_2 increment, especially for longer chains, and it was possible to reasonably reproduce the theoretical (DFT) vibrational frequencies by employing a force field as implied by Figure 1 (α- and β-carbons/hydrogens only). For fixing the force-field parameters, the simpler models of Jørgensen et al.[59] and Böhm et al.[60] served as starting points. To achieve a better agreement of especially the low-frequency part of the vibrational spectrum with theoretical/experimental values, substantial parameter changes had to be made. The resultant parameter set for bond, angle, and dihedral potentials is collected in Table 6. In addition to CC−CC torsional potentials, HC−CH torsions had to be included. Despite the small amplitudes, A, of respective cosine-type dihedral potentials (cf. Table 6), their omission would lead to significant changes in the normal-mode spectra. The force-field parameters of the ether and thioether groups were taken from the standard CHARMM force field.[61] Finally, the force-field

TABLE 6: Force Field of the Alkyl Chain[a]

Bonds		
	k_r [kcal/(mol Å^2)]	r_0 (Å)
$C_\alpha-C_\beta$	330.0	1.508
$C_\beta-C_\beta$	330.0	1.508
$H_\alpha-C_\alpha$	360.0	1.093
$H_\beta-C_\beta$	340.0	1.093
Angles		
	k_θ [kcal/(mol rad^2)]	θ_0 (deg)
$C_\alpha-C_\beta-C_\beta$	60.0	109.1
$C_\beta-C_\beta-C_\beta$	60.0	109.1
$H_\alpha-C_\alpha-H_\alpha$	80.0	108.7
$H_\beta-C_\beta-H_\beta$	80.0	108.4
$H_\alpha-C_\alpha-C_\beta$	80.0	110.3
$H_\beta-C_\beta-C_\alpha$	80.0	109.8
$H_\beta-C_\beta-C_\beta$	80.0	109.8
Dihedrals		
	A (kcal/mol)	m	δ (deg)
$H_\alpha-C_\alpha-C_\beta-H_\beta$	0.2	3	0.0
$H_\beta-C_\beta-C_\beta-H_\beta$	0.2	3	0.0
$C_\alpha-C_\beta-C_\beta-C_\beta$	8.0	3	0.0
$C_\beta-C_\beta-C_\beta-C_\beta$	8.0	3	0.0

[a] Potential energy functions have the forms $V(r) = 0.5k_r(r - r_0)^2$, $V(\theta) = 0.5k_\theta(\theta - \theta_0)^2$, and $V(\Phi) = A[1 + \cos(m\Phi - \delta)]$ for the bonds, angles, and dihedral angles, respectively.

parameters for interactions at the azulene−alkyl and alkyl−anthracene interfaces are summarized in Table 7. There, the atom types are assigned superscript indexes (azu, ant, alk) indicating the molecular subunit to which they belong, whereas the Greek subscript indexes indicate the corresponding atom type within the respective subunit. As mentioned earlier, the interfacial force-field parameters were considered to be independent of the alkyl chain length in light of the agreement with the theoretical (DFT) vibrational spectra.

The complete force field for the alkyl-bridged bichromophoric compounds as described above was adapted to the normal-mode

TABLE 7: Force Field for the azu−alk and alk−ant Interfaces[a]

Bonds		
	k_r [kcal/(mol Å^2)]	r_0 (Å)
$C_\beta^{azu}-C_\alpha^{alk}$	330.0	1.504
$C_\alpha^{alk}-C_\delta^{ant}$	330.0	1.518
Angles		
	k_θ [kcal/(mol rad^2)]	θ_0 (deg)
$H_\alpha^{alk}-C_\alpha^{alk}-C_\beta^{azu}$	40.0	109.6
$C_\alpha^{azu}-C_\beta^{azu}-C_\alpha^{alk}$	40.0	125.3
$C_\gamma^{azu}-C_\beta^{azu}-C_\alpha^{alk}$	40.0	127.2
$C_\beta^{azu}-C_\alpha^{alk}-C_\beta^{alk}$	40.0	113.2
$H_\alpha^{alk}-C_\alpha^{alk}-C_\delta^{ant}$	40.0	109.6
$C_\beta^{alk}-C_\alpha^{alk}-C_\delta^{ant}$	40.0	115.1
$C_\alpha^{alk}-C_\delta^{ant}-C_\gamma^{ant}$	40.0	120.3
Dihedrals		
	A (kcal/mol)	m	δ (deg)
$C_\alpha^{azu}-C_\beta^{azu}-C_\alpha^{alk}-C_\beta^{alk}$	2.4	2	0.0
$C_\beta^{alk}-C_\beta^{alk}-C_\alpha^{alk}-C_\delta^{ant}$	4.8	3	0.0
$C_\gamma^{azu}-C_\beta^{azu}-C_\alpha^{alk}-C_\beta^{alk}$	2.4	2	0.0
$C_\beta^{azu}-C_\alpha^{alk}-C_\beta^{alk}-C_\beta^{alk}$	4.8	3	0.0
$C_\beta^{alk}-C_\alpha^{alk}-C_\delta^{ant}-C_\gamma^{ant}$	2.8	2	0.0

[a] Potential energy functions have the forms $V(r) = 0.5k_r(r - r_0)^2$, $V(\theta) = 0.5k_\theta(\theta - \theta_0)^2$, and $V(\Phi) = A[1 + \cos(m\Phi - \delta)]$ for the bonds, angles, and dihedral angles, respectively.

spectrum only, which was calculated at a particular (all-trans) conformation of the flexible alkyl chain unit. As a result, it is expected to provide a fairly good description of the potential energy surface only in the neighborhood of the (respective) energy minimum. Whereas the quadratic bond stretch potentials are purely quadratic in Cartesian space, the quadratic angle, dihedral, and cosine-type dihedral potentials are not and thus produce anharmonic couplings among the vibrational normal modes mediating IVR. As noted earlier, these anharmonic couplings are "accidental" (uncontrolled) but nevertheless considered physically realistic. For later reference, we mention here that substituting the quadratic bond stretch functions by Morse potentials did not significantly influence the simulated IVR.

A disadvantage of the current force field is the energetic equivalence of trans and gauche conformations, which does not allow for a proper description of folded chain structures. Because of the large CC−CC torsional barriers however, the all-trans conformation was kinetically stable during the simulated physical time window of 150 ps, as it should be. The kinetic stability of the all-trans chain conformation also made it possible to analyze the energy-transfer process in terms of vibrational normal modes defined relative to the all-trans energy minimum.

References and Notes

(1) Owrutsky, J. C.; Raftery, D.; Hochstrasser, R. M. *Annu. Rev. Phys. Chem.* **1994**, *45*, 519.
(2) Egorov, S. A.; Skinner, J. L. *J. Chem. Phys.* **1996**, *105*, 7047.
(3) Heidelbach, C.; Vikhrenko, V. S.; Schwarzer, D.; Schroeder, J. *J. Chem. Phys.* **1999**, *110*, 5286.
(4) Schwarzer, D.; Hanisch, C.; Kutne, P.; Troe, J. *J. Phys. Chem. A* **2002**, *106*, 8019.
(5) Elles, C. G.; Bingemann, D.; Heckscher, M. M.; Crim, F. F. *J. Chem. Phys.* **2003**, *118*, 5587.
(6) von Benten, R.; Link, O.; Abel, B.; Schwarzer, D. *J. Phys. Chem. A* **2004**, *108*, 363.
(7) Gilbert, R. G.; Smith, S. C. *Theory of Unimolecular and Recombination Reactions*; Blackwell Scientific: Oxford, U.K., 1990.
(8) Baer, T.; Hase, W. L. *Unimolecular Reaction Dynamics*; Oxford University Press: New York, 1996.
(9) Hu, X.; Hase, W. L. *J. Phys. Chem.* **1989**, *93*, 6029.
(10) Sekiguchi, K.; Shimojima, A.; Kajimoto, O. *Chem. Phys. Lett.* **2002**, *356*, 84.
(11) Aβmann, J.; Charvat, A.; Schwarzer, D.; Kappel, C.; Luther, K.; Abel, B. *J. Phys. Chem. A* **2002**, *106*, 5197.
(12) Käb, G.; Schröder, C.; Schwarzer, D. *Phys. Chem. Chem. Phys.* **2002**, *4*, 271.
(13) Quack, M. *Annu. Rev. Phys. Chem.* **1990**, *41*, 839.
(14) Heidelbach, C.; Schroeder, J.; Schwarzer, D.; Vikhrenko, V. S. *Chem. Phys. Lett.* **1998**, *291*, 333.
(15) Felker, P. M.; Zewail, A. H. *Phys. Rev. Lett.* **1984**, *53*, 501.
(16) Geers, A.; Kappert, J.; Temps, F.; Wiebrecht, J. W. *J. Chem. Phys.* **1994**, *101*, 3618.
(17) Timbers, P. J.; Parmenter, C. S.; Moss, D. B. *J. Chem. Phys.* **1994**, *100*, 1028.
(18) Schwarzer, D.; Kutne, P.; Schröder, C.; Troe, J. *J. Chem. Phys.* **2004**, *121*, 1754.
(19) Botan, V.; Backus, E. H. G.; Pfister, R.; Moretto, A.; Crisma, M.; Toniolo, C.; Nguyen, P.; Stock, G.; Hamm, P. *Proc. Nat. Acad. Sci.* **2007**, *104*, 12749.
(20) Carter, J. A.; Wang, Z.; Dlott, D. D. *J. Phys. Chem. A* **2008**, *112*, 3523.
(21) Schwarzer, D.; Troe, J.; Schroeder, J. *Ber. Bunsen-Ges. Phys. Chem.* **1991**, *95*, 933.
(22) Ruth, A. A.; Kim, E.-K.; Hese, A. *Phys. Chem. Chem. Phys.* **1999**, *1*, 5121.
(23) Kutne, P. Zeitaufgelöste Untersuchungen zum intramolekularen Schwingungsenergiefluss durch molekulare Ketten, Ph.D. Thesis, Georg-August Universität Göttingen, Göttingen, Germany, 2003.
(24) Fourier, J. Théorie analytique de la chaleur. Reprinted in *Oeuvres*; Gauthiers-Villars: Paris, 1888.
(25) Lepri, S.; Livi, R.; Politi, A. *Phys. Rep.* **2003**, *377*, 1.
(26) Segal, D.; Nitzan, A.; Hänggi, P. *J. Chem. Phys.* **2003**, *119*, 6840.
(27) Pollack, G. L. *Rev. Mod. Phys.* **1969**, *41*, 48.
(28) Swartz, E. T.; Pohl, R. O. *Rev. Mod. Phys.* **1989**, *61*, 605.
(29) Watanabe, T.; Ni, B.; Phillpot, S. R.; Schelling, P. K.; Keblinski, P. *J. Appl. Phys.* **2007**, *102*, 063503.
(30) Huang, Z.; Tang, Z. *Physica B* **2006**, *373*, 291.
(31) Schelling, P. K.; Phillpot, S. R.; Keblinksi, P. *Phys. Rev. B* **2002**, *65*, 144306.
(32) Tang, Q. *Mol. Phys.* **2004**, *102*, 1959.
(33) Mahan, G. D. *Phys. Rev. B* **2009**, *79*, 075408.
(34) Krenzer, B.; Hanisch, A.; Duvenbeck, A.; Rethfeld, B.; Horn-von Hoegen, M. *J. Nanomater.* **2008**, 1.
(35) Rohsenow, W. M.; Hartnett, J. P.; Cho, Y. I. *Handbook of Heat Transfer*; McGraw-Hill: New York, 1998.
(36) Baehr, H. D.; Stephan, K. *Heat and Mass Transfer*; Springer-Verlag: Berlin, 1998.
(37) McQuarrie, D. A. *Statistical Mechanics*; Harper and Row: New York, 1976.
(38) Zwanzig, R. *Nonequilibrium Statistical Mechanics*; Oxford University Press: New York, 2001.
(39) Schröder, C. Molekulardynamische Simulationen zum intra- und intermolekularen Schwingungsenergietransfer von ausgewählten Molekülen. Ph.D. Thesis, Georg-August Universität Göttingen, Göttingen, Germany, 2003.
(40) Lamoureux, G.; Roux, B. *J. Chem. Phys.* **2003**, *119*, 3025.
(41) Harvey, S. C.; Tan, R. K.-Z.; Cheatham, T. E., III. *J. Comput. Chem.* **1998**, *19*, 726.
(42) Gonzalez-Luque, R.; Garavelli, M.; Bernardi, F.; Merchán, M.; Robb, M. A.; Olivucci, M. *Proc. Natl. Acad. Sci. U.S.A.* **2000**, *97*, 9379.
(43) Vreven, T.; Morokuma, K. *J. Chem. Phys.* **2000**, *113*, 2969.
(44) Müller-Plathe, F. *J. Chem. Phys.* **1997**, *106*, 6082.
(45) Kim, B. H.; Beskok, A.; Cagin, T. *Microfluidics Nanofluidics* **2008**, *5*, 551.
(46) Maiti, A.; Mahan, G. D.; Pantelides, S. T. *Solid State Commun.* **1997**, *102*, 517.
(47) Saslow, W. M. *Phys. Rev. B* **1975**, *11*, 2544.
(48) Mergenthaler, D. B.; Pietralla, M. *Z. Phys. B* **1994**, *94*, 461.
(49) Schelling, P. K.; Phillpot, S. R. *J. Am. Ceram. Soc.* **2001**, *84*, 2997.
(50) Dhar, A. *Phys. Rev. Lett.* **2001**, *86*, 5882.
(51) Rieder, Z.; Lebowitz, J. L.; Lieb, E. *J. Math. Phys.* **1967**, *8*, 1073.
(52) Frisch, M. J.; Trucks, G. W.; Schlegel, H. B.; Scuseria, G. E.; Robb, M. A.; Cheeseman, J. R.; Zakrzewski, V. G.; Montgomery, J. A.,

Jr.; Stratmann, R. E.; Burant, J. C.; Dapprich, S.; Millam, J. M.; Daniels, A. D.; Kudin, K. N.; Strain, M. C.; Farkas, O.; Tomasi, J.; Barone, V.; Cossi, M.; Cammi, R.; Mennucci, B.; Pomelli, C.; Adamo, C.; Clifford, S.; Ochterski, J.; Petersson, G. A.; Ayala, P. Y.; Cui, Q.; Morokuma, K.; Malick, D. K.; Rabuck, A. D.; Raghavachari, K.; Foresman, J. B.; Cioslowski, J.; Ortiz, J. V.; Baboul, A. G.; Stefanov, B. B.; Liu, G.; Liashenko, A.; Piskorz, P.; Komaromi, I.; Gomperts, R.; Martin, R. L.; Fox, D. J.; Keith, T.; Al-Laham, M. A.; Peng, C. Y.; Nanayakkara, A.; Gonzalez, C.; Challacombe, M.; Gill, P. M. W.; Johnson, B.; Chen, W.; Wong, M. W.; Andres, J. L.; Head-Gordon, M.; Replogle, E. S.; Pople, J. A. *Gaussian 98*, revision A.1x; Gaussian Inc.: Pittsburgh, PA, 1998.

(53) Wong, M. W. *Chem. Phys. Lett.* **1996**, *256*, 391.

(54) Goodman, J. M. *J. Chem. Inf. Comput. Sci.* **1997**, *37*, 876.

(55) Allinger, N. L.; Yuh, Y. H.; Lii, J. H. *J. Am. Chem. Soc.* **1989**, *111*, 8551.

(56) Heidelbach, C.; Fedchenia, I. I.; Schwarzer, D.; Schroeder, J. *J. Chem. Phys.* **1998**, *108*, 10152.

(57) Chakraborty, D.; Ambashta, R.; Manogaran, S. *J. Phys. Chem.* **1996**, *100*, 13963.

(58) Halgren, T. A. *J. Comput. Chem.* **1996**, *17*, 490.

(59) Jørgensen, W. L.; Madura, J. D.; Swenson, C. J. *J. Am. Chem. Soc.* **1984**, *106*, 6638.

(60) Böhm, H. J.; Ahlrichs, R.; Scharf, P.; Schiffer, H. *J. Chem. Phys.* **1984**, *81*, 1389.

(61) Brooks, B. R.; Bruccoleri, R. E.; Olafson, B. D.; States, D. J.; Swaminathan, S. *J. Comput. Chem.* **1983**, *4*, 187.

JP903546H